Data-driven estimated velocity and pressure fields using snapshot PIV and fast probes

Junwei Chen*, Marco Raiola, Stefano Discetti[1]

Aerospace Engineering Research Group, Universidad Carlos III de Madrid, Spain
*Corresponding author: junwei.chen@uc3m.es

Keywords: Data-driven methods, Pressure estimation, Extended Proper Orthogonal Decomposition, Neural networks.

ABSTRACT

In this article, the time-resolved flow field estimation based on data-driven methods, which exploits the measurement of snapshot PIV and probes working at high frequency, is introduced as a pathway to obtain pressure fields from non-time resolved measurements. Time-resolved velocity fields are reconstructed from the combination of a large number of uncorrelated velocity fields and time-resolved data from velocity probes sampled in few points in space. Using the estimated time-resolved velocity fields, the pressure field is obtained from integration of the pressure gradient from the Navier-Stokes equation without any further model for the time-derivative of the velocity. Extended Proper Orthogonal Decomposition (Extended POD), which builds the relation between flow fields and probe data from their temporal modes, is demonstrated in this paper to show the feasibility of this concept. Additionally, flow field estimation using a Multilayer Perceptron (MLP) with time-delay embedding is tested. This kind of estimator can map non-linear relations between probe and field data, at the expense of higher complexity and computational cost. The performances of both data-driven methods as well as Taylor's hypothesis are tested on a synthetic dataset, i.e. the numerical simulation of the wake of a fluidic pinball, and experimental measurements on the wake of a wing. The tests show that both data-driven methods estimate the velocity and pressure field with sufficient accuracy. In the cases analyzed in this paper, both having compact POD spectra, the data-driven methods outperform the estimation based on Taylor's hypothesis. As an additional benefit, after training, the data-driven methods only require data from probe to estimate the flow fields.

1. Introduction

The pressure field can be extracted from time-resolved PIV (Particle Image Velocimetry) data by enforcing the Navier-Stokes equation (Van Oudheusden, 2013). The pressure gradient can be re-stated as a function of the velocity as in the following,

$$\nabla p = \mathbf{f}(\mathbf{u}) = -\rho\frac{D\mathbf{u}}{Dt} + \mu\nabla^2\mathbf{u} \tag{1}$$

where ρ and μ is the density and dynamic viscosity of fluid, ∇ is the gradient operator, and the material derivative $D\mathbf{u}/Dt$ can be expressed in the Eulerian way as $\partial\mathbf{u}/\partial t + (\mathbf{u}\cdot\nabla)\mathbf{u}$. This emphasizes the importance of time derivative of velocity in the estimation of pressure. The most direct way to obtain the time derivatives is by having access to time-series of the velocity field obtained through high-repetition rate PIV. However, the limitation in the sampling rate of available imaging and illumination systems and their high price tag, restrict the access to time-resolved PIV for most experimental studies. Moreover, the operations of temporal or spatial derivative amplify the noise, thus even when the velocity field from PIV are moderately good, the pressure field integrated from its gradient can have large degree of errors with respect to the real one. This requires high accuracy for the velocity field.

To solve the first issue, some assumptions can be applied to estimate the time-derivative of the velocity from a single snapshot when the time resolution is not available, such as Taylor's hypothesis (TH) (Van der Kindere et al., 2019), or non-dissipative vortex advection (Schneiders et al., 2018). Another approach is to bypass the time derivative completely by reformulating Eq. 1 as a Poisson problem and assuming that the flow is incompressible,

$$\nabla^2 p = -\rho\nabla\cdot(\mathbf{u}\cdot\nabla)\mathbf{u} \tag{2}$$

However, even in this approach the time derivative is typically still required on the boundary of the domain, thus needing additional assumptions there.

An alternative path to access time-resolved measurements is offered by estimation of fields using sensors. Normally point probes (such as hot-wires or microphone) provide easily time-resolved measurement at a reasonable cost, at the expense of spatial resolution. We have recently demonstrated that a combined use of non-time-resolved PIV measurements and time-resolved probe measurements can be enforced to obtain pressure fields from integration of estimated velocity fields. The technique used by Chen et al. (2022) roots in the Extended Proper Orthogonal Decomposition (Extended POD) (Borée, 2003). Probe data are used as encoders for the field information, thus retrieving time-resolved velocity fields using probes. After training, this method only requires probe data to obtain velocity and pressure field in the entire domain of training. The entire process is summarized in Fig. 1.

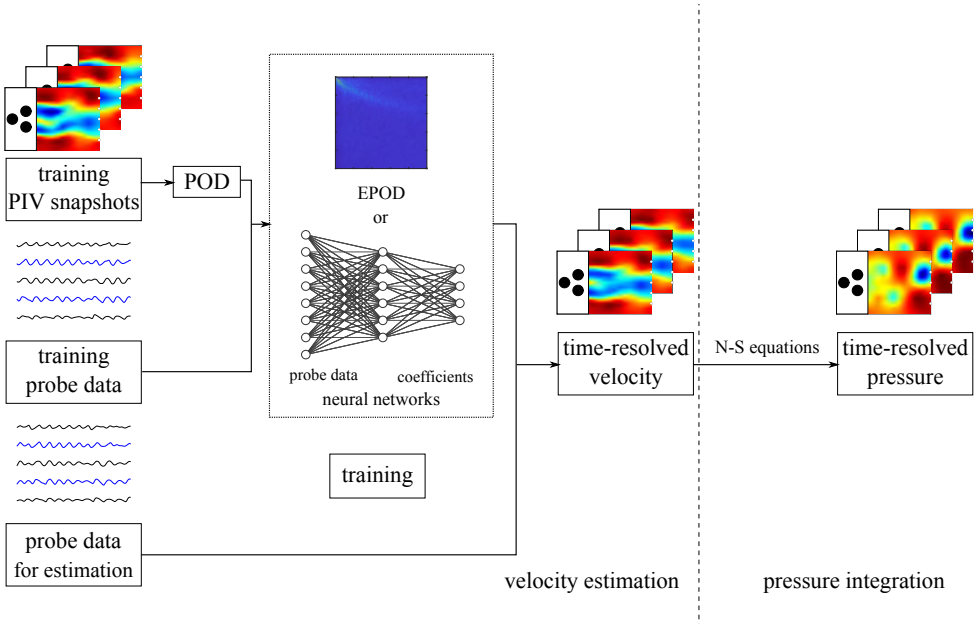

Figure 1. Flow chart of data-driven velocity estimation and pressure integration. Adapted from Chen et al. (2022).

In this work, we revise the performances of this method and compare it to an enhanced version based on a non-linear estimator of the flow fields. Deep learning architectures have widely demonstrated their suitability for this task (Güemes et al., 2019; Erichson et al., 2020; Giannopoulos & Aider, 2020; Guastoni et al., 2021; Manohar et al., 2022). Such estimator seeks to encode the probe data into the POD temporal coefficients of the fields to be estimated. The estimation methods will be described first in Sec. 2. The methodology is then assessed on a synthetic test case of the wake of a fluidic pinball (Sec. 3) and an experiment on the wake of a wing (Sec. 4).

2. Velocity field reconstruction methods

2.1. Estimation of time-resolved velocity fields with Extended POD

In this section the data arrangement and the implementation of the EPOD-based method for the estimation of velocity fields from point probes is presented. The treatment follows the formulation presented in (Discetti et al., 2018). It is worth to remark that this approach, although defined in the time-domain, is equivalent to a multi-time delay Linear Stochastic Estimation (Ewing & Citriniti, 1999; Tinney et al., 2006).

Assume that n_t snapshots of the fluctuating velocity field are arranged into a matrix U, where each row (with length $n_p \times 2$ for planar PIV) contains the velocity components in all the nodes of the domain. The matrix U can be decomposed by the economy-size Singular Value Decomposition (SVD), i.e.

$$U = \Psi \Sigma \Phi^T \tag{3}$$

For simplicity it is herein assumed that all grid points cover the same area, thus there is no need to explicitly include a weighting matrix. Furthermore we assume $n_t < 2n_p$. Both conditions are normally met in PIV experiments. Nonetheless, the method can be easily formulated for the general case of non-uniform spatial resolution and/or $n_t > 2n_p$. In the decomposition of Eq. 3, the columns of the $n_t \times n_t$ orthogonal matrix Ψ contains the temporal modes ψ_i, the columns of the $n_t \times 2n_p$ orthogonal matrix Φ^T contains the spatial modes ϕ_i and Σ is a square diagonal matrix containing the singular values σ_i arranged in a decreasing order.

The same decomposition can be applied on velocity data from s probes synchronized with velocity field measurements. The data from the probes extracted at the same time instants of the PIV measurements can be arranged in a snapshot matrix, with dimension $n_t \times (s \times n_c)$, with n_c being the number of components measured by the probe. In order to increase the quantity of probe data available for each snapshot, a multi-time-delay embedding approach, analogous to the one adopted in (Sicot et al., 2012; Hosseini et al., 2015), is employed here: for each physical probe, a time-resolved sequence of q probe samples is extracted after the velocity field sampling time and considered as additional probes, referred for simplicity as "virtual probes". This approach is also known as Multichannel Singular Spectrum Analysis (Ghil et al., 2002). This method is in wide sense enforcing Taylor's hypothesis, although not explicitly including a model nor imposing a precise convection velocity. The final result is a multi-time delay embedding in the snapshot probe matrix. The final result is a matrix U_{pr} with n_t rows (as the velocity field snapshots) and $n_{tt} = (s \times n_c) \times q$ columns which can be decomposed as

$$U_{pr} = \Psi_{pr} \Sigma_{pr} \Phi_{pr}^T \tag{4}$$

The extended POD modes Φ_e corresponding to the field measurements can be estimated by projection of the PIV snapshot matrix U on the temporal modes of the probe, i.e.

$$\Psi_{pr}^T U = \Sigma_e \Phi_e^T = \Phi_{pr}^T \Psi \Sigma \Phi^T = \Xi \Sigma \Phi^T \tag{5}$$

where the subscript e refers to extended POD modes and the matrix $\Xi = \Psi_{pr}^T \Psi$ contains the information about the temporal correlation between field and probe modes.

Knowing the POD spatial modes (Φ and Φ_{pr}) and singular values (Σ and Σ_{pr}) of the velocity field and of the probe snapshot matrix, as well as the temporal correlations matrix Ξ, it is possible to estimate the velocity field u_{est} at an generic instant from a probe data snapshot u_{se} sampled at that instant:

$$u_{est} = u_{se} \Phi_{pr} \Sigma_{pr}^{-1} \Xi \Sigma \Phi^T = \psi_{est} \Sigma \Phi^T \tag{6}$$

with u_{se} containing delay-embedded probe data in the same arrangement used to construct the probe snapshot matrix.

Since the pressure gradient estimation heavily relies on a correct estimate of the time derivative of the velocity field, it is of utmost importance to reduce spurious noise in the reconstruction. For

this reason, a temporal smoothing of the estimate temporal modes is tested. In the present work a 6^{th} order low-pass Butterworth filter with cutoff frequency equal to 0.05 times the data sample rate is applied to each estimated temporal mode ψ_{est}. This approach has been referred to as ψ-*filtering* approach by Chen et al. (2022).

2.2. Estimation of time-resolved velocity fields with artificial neural networks

In order to extend the capabilities of the pressure-estimation method proposed by Chen et al. (2022), we introduce a non-linear estimator for the POD time coefficients. The relation between the probe data U_{pr} and the temporal modes of velocity fields Ψ is built with a multilayer perceptron (MLP). MLP is one of the basic forms of ANN, based on fully-connected layers. The fully-connected layers are composed of artificial neurons, performing weighted sums on neuron values from input or previous layers, and passing the summation through a activation function (usually non-linear) producing a single output. The values of weight are refined in training, using backpropagation algorithm. In our implementation the training data are the coefficients of spatial modes of the flow field and probe data in the same snapshot, thus the learning is supervised. The price to pay to build a non-linear estimator is an increase in computational cost and complexity with respect to EPOD.

After the training, the temporal modes of the flow field can be reconstructed by feeding the neural networks with the probe data of generic time instants. Also in this case, a low-pass filter can be applied to the temporal modes to improve the reconstruction quality.

3. Validation

In this section a validation using a synthetic dataset is carried out. The settings of the virtual experiment are the same adopted by Chen et al. (2022) and summarized here briefly.

The dataset has been extracted from a 2D-DNS (2 Dimensional Direct Numerical Simulation) of the wake of a *fluidic pinball* (Deng et al., 2020). The pinball is formed by three cylinders with diameter D, whose centres form an equilateral triangle with side length equal to $1.5D$. The triangle is oriented with one vertex pointing upstream. The 2D-DNS is performed at $Re = 130$ (referred as chaotic regime, (Deng et al., 2020)), with Re being the Reynolds number based on the freestream velocity and the diameter of the cylinders forming the pinball.

The region selected to test the EPOD-based estimation is placed in the wake of the obstacles, ranging from $x = 1D$ to $x = 7D$ and from $y = -3D$ to $y = 3D$, with x and y being respectively the streamwise and crosswise directions. The velocity data from the original DNS mesh are interpolated on a Cartesian grid with distance between two adjacent points of $0.08D$ in order to simulate the results of a PIV experiment, yielding 76×76 vector fields (although neither modulation nor random errors are introduced).

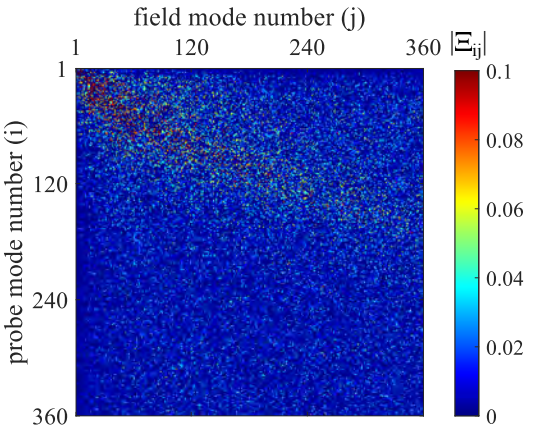

Figure 2. Absolute value of Ξ for the fluidic pinball case (first 360×360 entries).

Figure 3. MLP Setting for the pinball test.

layer	nodes	activation function
1	512	relu
2	512	relu
3	60	

Five point probes measuring the 2 in-plane components of velocity, are placed at the downstream edge of the region ($x = 7D$), with a spacing of $1D$ in the y direction, being the central one located at $y = 0$. The training dataset is composed of 4685 velocity field snapshots as well as of the synchronized virtual probe data, forming the matrices U and U_{pr}, respectively, as reported in Sec. 2.1. The snapshots are selected to have a temporal spacing of 1.9 non-dimensional times. The probes instead store data with the same time separation of the DNS time step, i.e. each 0.1 in non-dimensional time units. This corresponds to a target super-sampling by a factor of 19. When building the probe snapshot matrix, a time segment equal to 60 samples is used. The number of virtual probes is estimated by considering a timespan covering the convection time through the observation domain, as proposed in (Discetti et al., 2018).

Fig. 2 shows the absolute value of the upper-left portion of unfiltered matrix Ξ, which is representative of the correlation between the i^{th} temporal mode of the probes and the j^{th} temporal mode of the flow field, with i and j being respectively the row and column numbers in Ξ. The matrix Ξ shows a clear diagonal dominance for at least the first 100 modes, which indicates a strong direct correspondence between probe and field modes. As the mode number is increased, this dominance disappears and each probe mode tends to correspond to a larger number of field modes.

The neural networks are trained on Google colab with one Tesla P100 GPU. The table reported in Fig. 3 illustrates the structure of the shallow neural network for the pinball test. The MLP contains 3 layers, with 512, 512 and 60 nodes, respectively. The *relu* activation functions is applied in the first two layers. The mean-square-error is applied as the lost function and the parameters of the neural networks are updated in the backpropagation to decrease the value of the loss function. The first 60 temporal modes, corresponding to 99.9% of the energy, are estimated with the MLP.

For completeness, the assessment includes also the pressure estimation based on enforcing Taylor's hypothesis, as in (Van der Kindere et al., 2019). This method enables the estimation of the time derivative of velocity, and thus of the pressure, for a measured snapshot. This approach will be referred to as *in-sample TH* in the remainder of this paper. A Gaussian spatial filter with standard

deviation equal to 7 vectors on a kernel of 29×29 vectors has been applied to the local velocity inside the measured snapshot to provide the convection velocity $\mathbf{u}_c$.

The performances of EPOD and MLP are reported in Fig. 4 for a single snapshot of the testing dataset, both in terms of velocity and of pressure. The velocity from DNS and pressure integrated from the velocity field using method in (Chen et al., 2022), normalized by the freestream velocity U_∞ or corresponding dynamic pressure $1/2\rho U_\infty^2$, are presented in the first row for comparison. In the second and third row, the velocity and pressure from ψ-filtered EPOD and ψ-filtered MLP are presented. The error of estimation via EPOD, MLP and TH in the same snapshot is presented in Fig. 5. Both EPOD and MLP reconstruct the velocity field and estimate the pressure field with relatively-high fidelity. MLP reconstructs almost exact velocity field, thus resulting in very good pressure estimation. The error of EPOD mainly affects the streamwise velocity component in the wake region (from $x = 2D$ to $x = 4D$), producing an error pattern which suggests the misplacement of flow structures in the y-direction. The crosswise velocity component and pressure shows lower levels of error, still localized in the same region. The region of the reconstruction error stands farther from the probe, thus hinting to the limited capability of estimating field data far from the probe locations. Additionally, the localization of such error might be an effect of the presence of intense flow features, strongly subjected to stretching and deformation, and for which the linear methods do not perform well. These two aspects contribute in the reduced capability of the probes to sense accurately the fluctuations in this region with linear methods such as EPOD. However, the capability of MLP to model non-linear mapping between probe and field data allows a significant reduction of this source of error.

A further quantitative assessment of the estimation error has been carried out over a testing dataset of 1500 snapshots by computing the Root Mean Square (RMS) error with respect to the original DNS fields. Additionally, the TH can be used to propagate the measured frame in time, obtaining an estimated time-resolved sequence of velocity fields. The simplest way to fulfill it is by means of a unidirectional Euler propagation, which is

$$\begin{aligned} \mathbf{u}(t_0 + dt) &= \mathbf{u}(t_0) + \left.\frac{\partial u}{\partial t}\right|_{t_0} dt \\ &= \mathbf{u}(t_0) - (\mathbf{u}_c \cdot \nabla)\mathbf{u}'(t_0)dt \end{aligned} \tag{7}$$

in the present case, where the convective velocity $\mathbf{u}_c$ is the spatially-filtered velocity inside the snapshot, and the time-resolved sequence has been estimated with TH using a 4^{th} order Runge-Kutta method with unidirectional propagation. This approach will be referred to as *out-of-sample TH* in the remainder of this paper. It should be noted that the error comes from both the absence of inlet information and the accumulation of that in propagation.

Fig. 6 shows the maps of estimation error for the unfiltered EPOD estimation (the first row), the ψ-filtered EPOD (the second row), the unfiltered MLP (the third row), the ψ-filtered MLP (the fourth row), and in-sample TH (in Fig. 7), where the RMS error of two-component velocity and their time-derivative, or pressure is calculated in all snapshots tested. The error of velocity is reported on the left column (Fig. 6a,d,g,j), and the error of the time-derivative of velocity is reported on

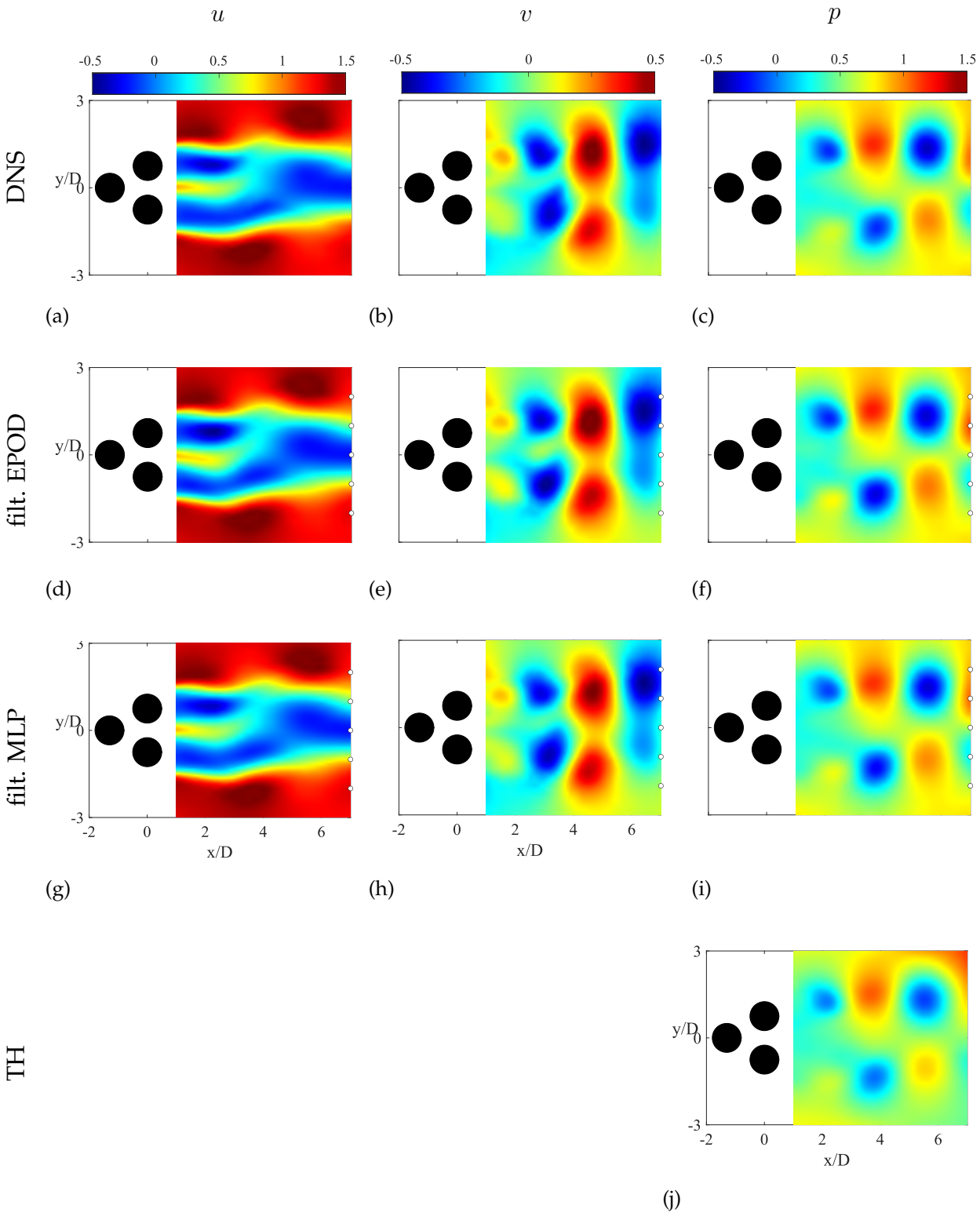

Figure 4. Exact and estimated velocity and pressure fields for a single snapshot: (**a**) streamwise velocity from DNS; (**b**) crosswise velocity from DNS; (**c**) pressure from DNS; (**d**) streamwise velocity from filtered EPOD; (**e**) crosswise velocity from filtered EPOD; (**f**) pressure from filtered EPOD; (**g**) streamwise velocity from filtered MLP; (**h**) crosswise velocity from filtered MLP; (**i**) pressure from filtered MLP; (**j**) pressure from TH.

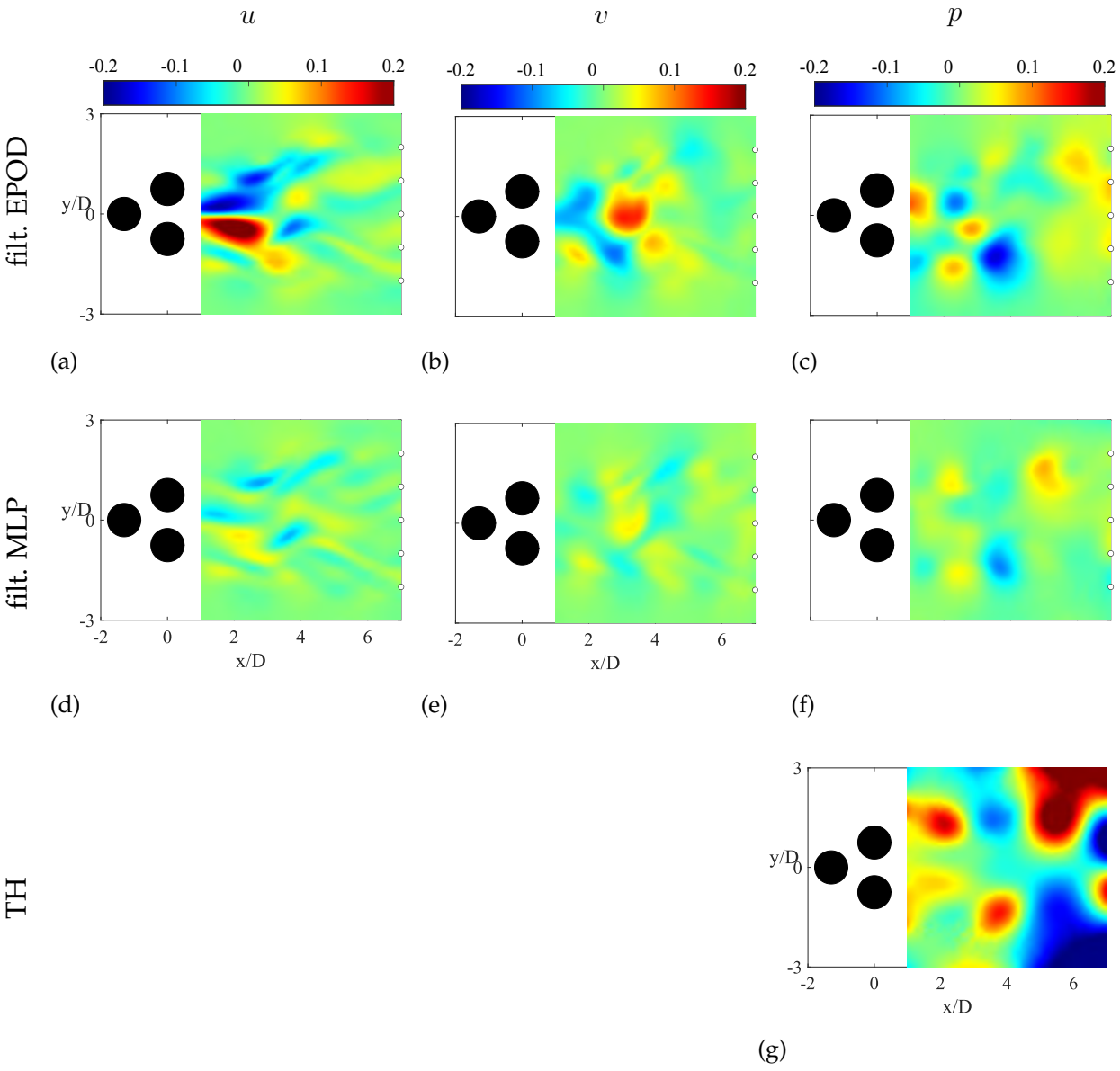

Figure 5. Error of estimated velocity and pressure fields for a single snapshot: (**a**) streamwise velocity from filtered EPOD; (**b**) crosswise velocity from filtered EPOD; (**c**) pressure from filtered EPOD; (**d**) streamwise velocity from filtered MLP; (**e**) crosswise velocity from filtered MLP; (**f**) pressure from filtered MLP; (**g**) pressure from TH.

the central column(Fig. 6b,e,h,k, Fig. 7a), and the error on the pressure on the right column(Fig. 6c,f,i,l, Fig. 7b). The in-sample TH is based on the assumption that exact velocity fields were available in all snapshot tested, thus only the time derivative of velocity is to be estimated. Despite the velocity estimation from the unfiltered EPOD (Fig. 6a) has reasonable levels of error, the pressure estimation (Fig. 6c) is affected by large error. Such error is mainly produced by the time derivative of the velocity (Fig. 6b), which also embodies in the spurious fluctuations in the POD temporal modes. The ψ-filter removes most of the error for the time-derivative, thus improves the pressure estimation significantly. It should be mentioned that time filtering may smear out high-frequency fluctuations. Nonetheless, such scales motions shift very fast and are less likely to exhibit correlation with the probe data, thus the estimation process is already partially filtering their intensity. The error of MLP shows significant improvement of velocity and their time-derivative even without filter, thus improving the pressure estimation, especially in the center region of the domain. A low-pass filter in time allow a minor improvement of the performance of MLP in the estimation of velocity, with a more significant reduction in the error in pressure estimation due to the integration process. Similar error levels of unfiltered EPOD are present in the pressure estimation from the TH (Fig. 7b), also in this case produced by large errors in the time derivative (Fig. 7a).

Since the frequency of data-driven methods in this article is based on the repetition rate of sensors, they can provide by default time-resolved flow fields. Taylor's hypothesis, by contrast, is generally employed to estimate the time-derivative from the velocity field within one snapshot (in-sample TH). The time-resolved flow field can be also derived by applying the unidirectional Euler propagation in 7, with the time-derivative from TH (out-of-sample TH), but the error increases rapidly due to lack of information between snapshots. To demonstrate it, the pressure estimation error along time from data-driven methods and in-sample/out-of-sample TH are shown in Fig. 8a. The out-of-sample TH on this figure propagates starting from the snapshots spacing in every $1/6$ non-dimensional through-time t^*, this non-dimensional amount in this article is defined as L/U_∞, where L is the domain length and U_∞ is the freestream velocity. the figure shows MLP is better than EPOD, the filter improves the estimation, and data-driven methods outperforms the TH in current case. The error of out-of-sample TH experiences three and half periods, with the error accumulates from the exact snapshot.

The robustness of the methods is tested given noise to the probe data of training and testing and field data of training. Gaussian noise with zero mean value and standard deviation up to 4% of U_∞ is superposed onto both velocity components. The RMS error of the pressure on all testing frames and the whole domain are shown on Fig. 8b, the out-of-sample TH has also the snapshot spacing at $1/6\Delta t^*$. The noise impacts the pressure estimation to all methods, thus the error increases for the model based method and in-sample TH, while the out-of-sample TH fails even the noise level is just 0.5%.

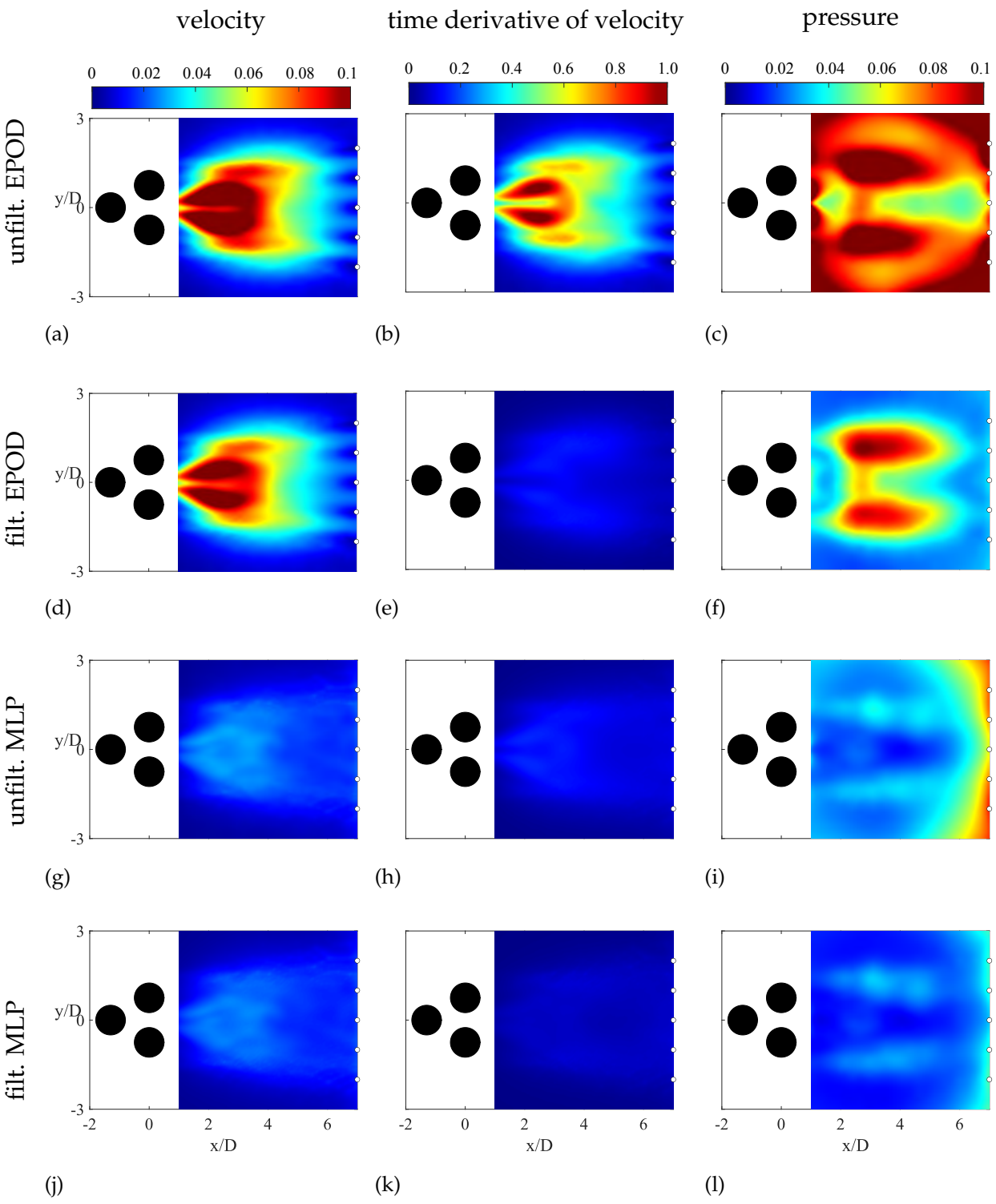

Figure 6. RMS error map of velocity and pressure fields estimation using the EPOD with and without filter, MLP with and without filter. The first column shows error on velocity, the second column shows error on time derivative, and the last column shows the error on pressure.

TH

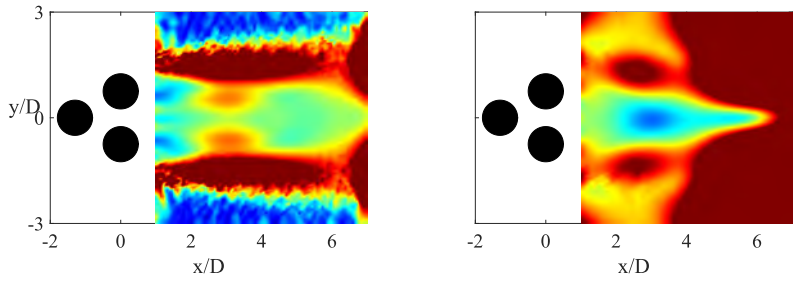

(a) (b)

Figure 7. Continuing Fig. 6, the RMS error of time derivative of velocity and pressure generated from TH.

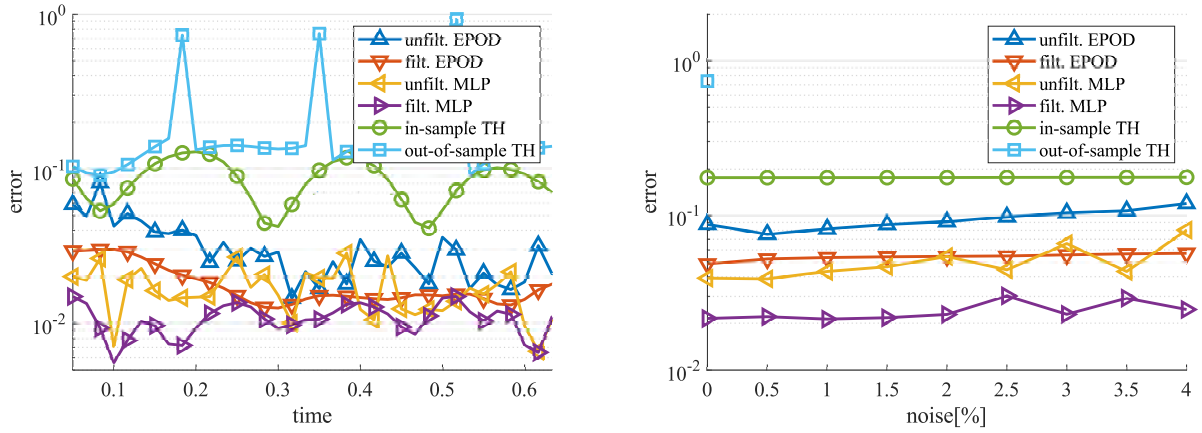

(a) (b)

Figure 8. (**a**) RMS error of estimated pressure over the whole domain as propagating in time, where the out-of-sample TH is propagated up to $\Delta t^* = 1/6$. (**b**) RMS error of estimated pressure over the whole domain for different levels of noise in probe data and training velocity field, the out-of-sample TH is the average in $\Delta t^* < 1/6$.

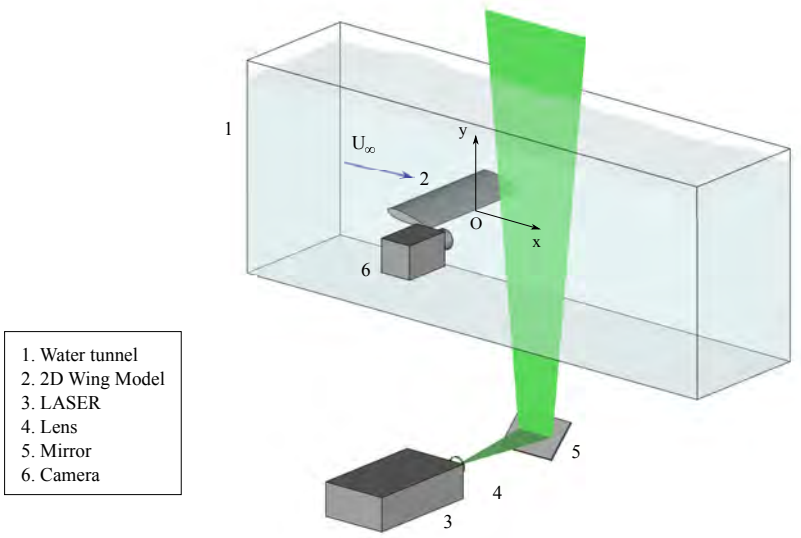

Figure 9. Sketch of experimental setting.

4. Experiments on the wake of wing

The proposed method is tested on an experimental dataset of a PIV measurement in the wake of a 2D wing with a NACA 0018 airfoil. The experiment is carried out in the water tunnel of the Universidad Carlos III de Madrid, which has a $2.5 \times 0.5 \times 0.55m^3$ test section. The Reynolds number is approximate 4800, with the chord length of the wing at $80mm$, and the freestream velocity at $U_\infty = 0.06m/s$. The wing is mounted with an angle of attack of $10°$ to generate a moderate-intensity shedding wake.

As shown in the sketch in Fig.9, a dual cavity pulsed Nd:YAG Quantel Evergreen laser is used to produce an approximately 1mm-thick sheet after reshaping the laser beam via a spherical and a cylindrical lens. An Andor sCMOS camera with $2560 \times 2160px^2$ sensor (with pixel pitch of 6.5 μm) is equipped with a 50mm focal length objective, and set to a resolution of $8.3px/mm$. The flow is seeded with neutrally-bouyant polymide particles with $56\mu m$ diameter. Particle images are sampled at $30Hz$, which is sufficient to obtain time-resolved measurements, being the particle displacement in the freestream within frames equal to approximately 16 pixels. A sliding correlation (Scarano & Moore, 2012) with 3-frame kernel is applied and the final interrogation window size is $40px$ with 75% overlap, resulting in a vector spacing of 1.20mm.

The training dataset for EPOD is composed of 1591 velocity fields captured at 2.72Hz, i.e. downsampling by a factor of 11 the original sequence. Artificial probes with higher temporal resolution are built by using the original sequence with sampling frequency at $30Hz$. This approach for testing is similar to the one proposed by Tu et al. (2013). The complete PIV domain spans $1.6c$ in the streamwise direction, starting at approximately $0.75c$ from the trailing edge. Eleven probes are set

on the downstream edge of the domain, and 100 records soon after the snapshot are extracted from the time series of probe data, to make the time span equal to one convective throughtime within the domain.

Both EPOD and MLP in Sec. 2 are tested to reconstruct the flow field from probe data. All temporal modes are reconstructed from EPOD. The MLP is trained to estimate the first 128 temporal modes. The MLP is made of a five-layers neural networks with 2048, 2048, 1024, 1024, and 128 nodes. Both temporal modes from EPOD and MLP are then low-pass filtered.

As a comparison, the in-sample and out-of-sample TH are tested, and the result of pressure estimation for one snapshot and RMS error over 980 frames are shown in Fig. 10. One snapshot pressure of the EPOD, MLP and in-sample TH result as well as pressure directly integrated from PIV field are shown in the left. MLP provides the best result, while EPOD shows reasonable estimations, but with significant contamination of random errors. In-sample TH predicts well in the centre of the domain, but the error is more significant near the edges of the domain. When propagating velocity fields with TH, the error on the pressure fields increases rapidly.

5. Conclusions

Fully data-driven approaches to estimate instantaneous pressure fields using snapshot PIV (i.e. without time resolution) and probe data have been presented and assessed. The velocity fields are estimated at the same time resolution of the probes using either EPOD or an artificial neural network, and the pressure gradient is integrated in space enforcing Navier-Stokes equation on the time-resolved flow field. After training, the estimation process only requires data from probes in input. The EPOD reconstructs the flow field leveraging the one-to-one relation of temporal modes between flow field and probe data, while the MLP builds a more complex non-linear mapping. Both approaches provide sufficient accuracy in estimating flow field. The MLP shows superior performance if compared to EPOD because it allows mapping of non-linear relations between probe and field data. On the downside, this approach has higher computational cost and requires careful training to avoid overfitting. Both methods outperform in most cases a pressure estimation based on Taylor's hypothesis, particularly in the flows with compact POD spectrum illustrated here.

Acknowledgements

This project has received funding from the European Research Council (ERC) under the European Union's Horizon 2020 research and innovation program (grant agreement No 949085). The authors warmly acknowledge N. Deng, B. Noack, M. Morzynski and L. Pastur for providing the code for the fluidic pinball simulations and A.Güemes for the experimental dataset.

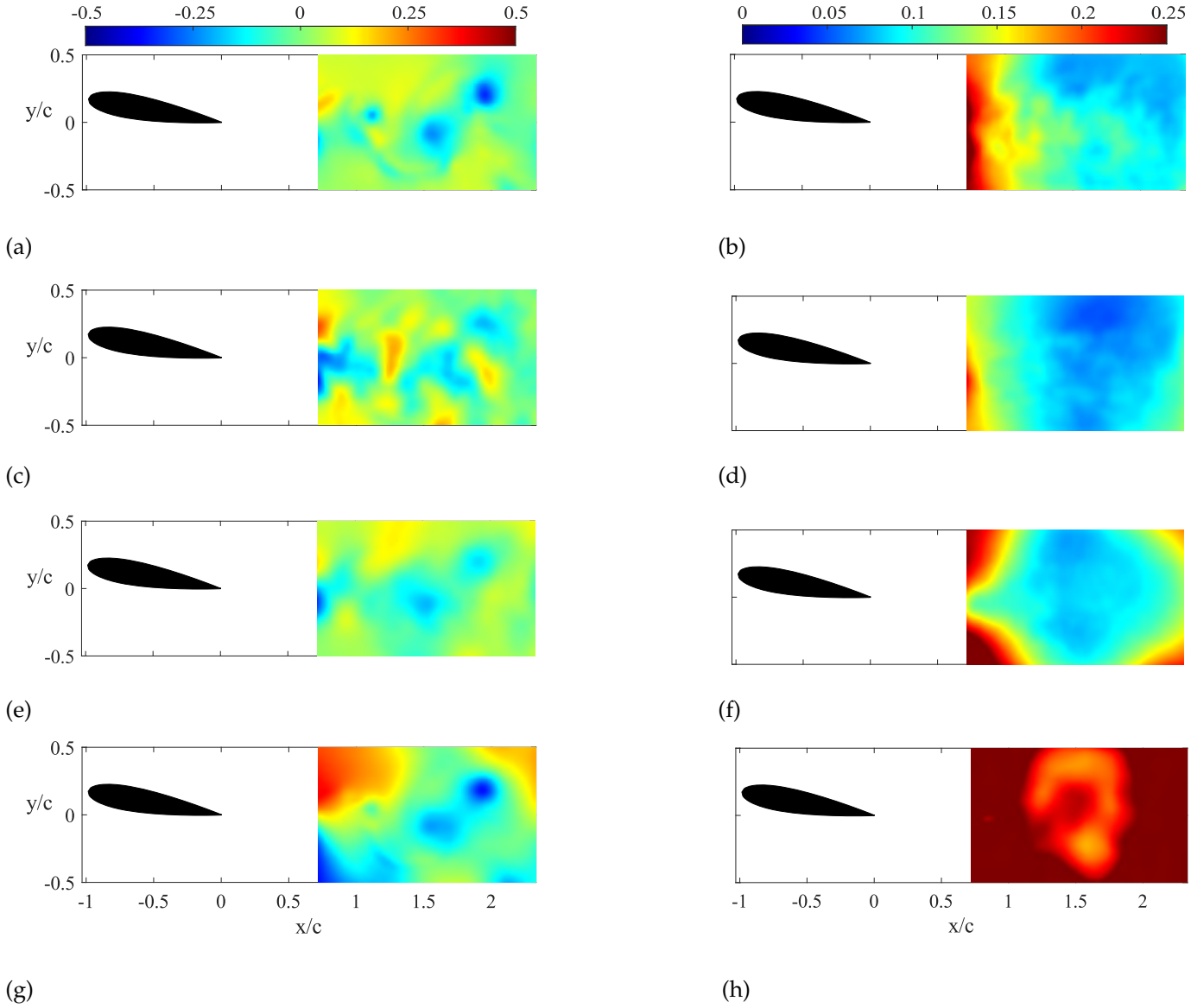

Figure 10. Non-dimensional instantaneous pressure field from: (**a**) time-resolved PIV; (**c**) EPOD reconstruction with filtering; (**e**) MLP reconstruction with filtering; (**g**) in-sample Taylor's hypothesis. Non-dimensional RMS error of pressure field from: (**b**) EPOD reconstruction with filtering; (**d**) MLP reconstruction with filtering; (**f**) in-sample Taylor's hypothesis; (**h**) out-of-sample Taylor's hypothesis, after the propagation of $0 \leq \Delta t^* < 0.25$ from sample snapshot.

References

Borée, J. (2003). Extended proper orthogonal decomposition: a tool to analyse correlated events in turbulent flows. *Experiments in Fluids*, *35*(2), 188–192.

Chen, J., Raiola, M., & Discetti, S. (2022). Pressure from data-driven estimation of velocity fields using snapshot piv and fast probes. *Experimental Thermal and Fluid Science*, *136*, 110647.

Deng, N., Noack, B. R., Morzyński, M., & Pastur, L. R. (2020). Low-order model for successive bifurcations of the fluidic pinball. *Journal of Fluid Mechanics*, *884*.

Discetti, S., Raiola, M., & Ianiro, A. (2018). Estimation of time-resolved turbulent fields through correlation of non-time-resolved field measurements and time-resolved point measurements. *Experimental Thermal and Fluid Science*, *93*, 119–130.

Erichson, N. B., Mathelin, L., Yao, Z., Brunton, S. L., Mahoney, M. W., & Kutz, J. N. (2020). Shallow neural networks for fluid flow reconstruction with limited sensors. *Proceedings of the Royal Society A*, *476*(2238), 20200097.

Ewing, D., & Citriniti, J. H. (1999). Examination of a LSE/POD complementary technique using single and multi-time information in the axisymmetric shear layer. In *Iutam symposium on simulation and identification of organized structures in flows* (pp. 375–384).

Ghil, M., Allen, M., Dettinger, M., Ide, K., Kondrashov, D., Mann, M., … others (2002). Advanced spectral methods for climatic time series. *Reviews of geophysics*, *40*(1), 3–1.

Giannopoulos, A., & Aider, J.-L. (2020). Prediction of the dynamics of a backward-facing step flow using focused time-delay neural networks and particle image velocimetry data-sets. *International Journal of Heat and Fluid Flow*, *82*, 108533.

Guastoni, L., Güemes, A., Ianiro, A., Discetti, S., Schlatter, P., Azizpour, H., & Vinuesa, R. (2021). Convolutional-network models to predict wall-bounded turbulence from wall quantities. *Journal of Fluid Mechanics*, *928*.

Güemes, A., Discetti, S., & Ianiro, A. (2019). Sensing the turbulent large-scale motions with their wall signature. *Physics of Fluids*, *31*(12), 125112.

Hosseini, Z., Martinuzzi, R. J., & Noack, B. R. (2015). Sensor-based estimation of the velocity in the wake of a low-aspect-ratio pyramid. *Experiments in Fluids*, *56*(1), 13.

Manohar, K. H., Morton, C., & Ziadé, P. (2022). Sparse sensor-based cylinder flow estimation using artificial neural networks. *Physical Review Fluids*, *7*(2), 024707.

Scarano, F., & Moore, P. (2012). An advection-based model to increase the temporal resolution of piv time series. *Experiments in Fluids*, *52*(4), 919–933.

Schneiders, J. F., Avallone, F., Pröbsting, S., Ragni, D., & Scarano, F. (2018). Pressure spectra from single-snapshot tomographic PIV. *Experiments in Fluids*, *59*(3), 57.

Sicot, C., Perrin, R., Tran, T., & Borée, J. (2012). Wall pressure and conditional flow structures downstream of a reattaching flow region. *International Journal of Heat and Fluid Flow*, *35*, 119–129.

Tinney, C., Coiffet, F., Delville, J., Hall, A., Jordan, P., & Glauser, M. (2006). On spectral linear stochastic estimation. *Experiments in Fluids*, *41*(5), 763–775.

Tu, J. H., Griffin, J., Hart, A., Rowley, C. W., Cattafesta, L. N., & Ukeiley, L. S. (2013). Integration of non-time-resolved PIV and time-resolved velocity point sensors for dynamic estimation of velocity fields. *Experiments in Fluids*, *54*(2), 1–20.

Van der Kindere, J., Laskari, A., Ganapathisubramani, B., & De Kat, R. (2019). Pressure from 2D snapshot PIV. *Experiments in Fluids*, *60*(2), 32.

Van Oudheusden, B. (2013). Piv-based pressure measurement. *Measurement Science and Technology*, *24*(3), 032001.